The ORFEO-GAIA and ORFEO-NMGRID Critical Heat Flux Correlations

ANP-10341NP
Revision 0

Topical Report

August 2016

AREVA Inc.

(c) 2016 AREVA Inc.

Copyright © 2016

AREVA Inc.
All Rights Reserved

Nature of Changes

Item	Section(s) or Page(s)	Description and Justification
1	All	Initial Issue

Contents

Page

1.0 INTRODUCTION 1-1
2.0 SUMMARY 2-1
2.1 ORFEO-GAIA CHF correlation 2-1
2.2 ORFEO-NMGRID CHF correlation 2-3
2.3 Correlations' application to the GAIA fuel assembly 2-4
3.0 REGULATORY REQUIREMENTS APPLICABLE TO THIS REPORT 3-1
4.0 CHF TESTING AND DATA 4-1
4.1 CHF test facilities 4-1
4.2 CHF test program 4-6
4.2.1 Test procedure and data collection methods 4-6
4.2.2 Test assembly configurations 4-10
4.2.3 CHF test program design – mixing grid 4-20
4.2.4 CHF test program design – non-mixing grid 4-22
4.2.5 Data collection ranges 4-24
4.3 CHF test data 4-24
5.0 SUBCHANNEL CODE 5-1
6.0 CORRELATION DEVELOPMENT 6-1
6.1 Background 6-1
6.2 ORFEO CHF correlation form 6-3
6.3 ORFEO-GAIA CHF correlation 6-17
6.4 ORFEO-NMGRID CHF correlation 6-22
6.5 Correlation behavior 6-27
7.0 CORRELATION ASSESSMENT AND STATISTICAL ANALYSIS 7-1
7.1 ORFEO-GAIA CHF correlation 7-1
7.1.1 Analysis of defining and validation data sets 7-1
7.1.2 Design limit 7-9
7.1.3 [ ] 7-23
7.1.4 Application range 7-28
7.2 ORFEO-NMGRID CHF correlation 7-32
7.2.1 Analysis of defining and validation data sets 7-32

7.2.2 Design limit 7-39
7.2.3 Application range 7-50
7.2.4 Application to the mixing grid CHF data set 7-54

8.0 GEOMETRIC COMPARISON OF PRODUCTION GRID TO TESTED GRID 8-1

9.0 QUALITY ASSURANCE PROGRAM (QAP)..... 9-1

9.1 QAP specific to correlation development 9-1

9.2 QAP specific to GAIA CHF testing 9-1

10.0 REFERENCES 10-1

APPENDIX A AXIAL GEOMETRY OF TEST ASSEMBILES ……..…….....A-1

APPENDIX B CHF TEST DATA ……..…….....B-1

APPENDIX C CORRELATION FITTING PROCESS ……..……..... C-1

List of Tables

Table 2-1 Key statistical parameters of the ORFEO-GAIA correlation 2-1
Table 2-2 Range of application for ORFEO-GAIA correlation (local thermal-hydraulic conditions) 2-1
Table 2-3 Geometry for ORFEO-GAIA correlation (fuel assembly geometry) 2-2
Table 2-4 Key statistical parameters of the ORFEO-NMGRID correlation 2-3
Table 2-5 Range of application for ORFEO-NMGRID correlation (local thermal-hydraulic conditions) 2-3
Table 2-6 Geometry for ORFEO-NMGRID correlation (fuel assembly geometry) 2-4
Table 4-1 Overall statistic results for test facilities benchmark 4-2
Table 4-2 KATHY test loop uncertainties 4-5
Table 4-3 Maximum deviations of CHF test parameters from nominal values 4-8
Table 4-4 Maximum deviations of CHF test parameters from [ ] 4-8
Table 4-5 Maximum deviations of CHF test parameters from [ ] 4-8
Table 4-6 Radial power factors for the mixing grid tests 4-16
Table 4-7 Radial power factors for the non-mixing grid tests 4-18
Table 4-8 Mixing grid CHF tests 4-21
Table 4-9 Non-mixing grid CHF tests 4-23
Table 5-1 Empirical correlations and numerical solution methods used in the COBRA-FLX subchannel code model 5-2
Table 6-1 Coefficients in F_{BASE} term 6-12
Table 6-2 Coefficients in FNU term 6-16
Table 6-3 Number of statepoints in the defining and validation data sets for ORFEO-GAIA correlation 6-18
Table 6-4 Coefficients in F_{SPACER} term for ORFEO-GAIA correlation 6-22
Table 6-5 Number of statepoints in the defining and validation data sets for ORFEO-NMGRID correlation 6-23
Table 6-6 Coefficients in F_{SPACER} term for ORFEO-NMGRID correlation 6-27
Table 7-1 Results of statistical tests applied to the defining and validation data sets for ORFEO-GAIA correlation 7-2
Table 7-2 Overall statistics of the defining and validation data sets for the ORFEO-GAIA correlation 7-4

Table 7-3 Overall statistics of the combined data set for the ORFEO-GAIA correlation 7-8
Table 7-4 Statistical parameters and design limit for ORFEO-GAIA correlation 7-13
Table 7-5 Distribution of statepoints below the ORFEO-GAIA correlation design limit by pressure ranges 7-14
Table 7-6 Distribution of statepoints below the ORFEO-GAIA correlation design limit by mass flux ranges 7-14
Table 7-7 Distribution of statepoints below the ORFEO-GAIA correlation design limit by equilibrium quality ranges 7-15
Table 7-8 Overall statistics of the combined data set for the ORFEO-GAIA correlation by subchannel type 7-17
Table 7-9 Overall statistics of the combined data set for the ORFEO-GAIA correlation by axial power profile type 7-17
Table 7-10 Overall statistics of the combined data set for the ORFEO-GAIA correlation by grid type 7-17
Table 7-11 Results of statistical tests applied to ORFEO-GAIA combined data set (subchannel, axial power profile and grid type) 7-18
Table 7-12 Range of application for ORFEO-GAIA CHF correlation (local thermal-hydraulic conditions) 7-31
Table 7-13 Results of statistical tests applied to the defining and validation data sets for ORFEO-NMGRID correlation 7-32
Table 7-14 Overall statistics of the defining and validation data sets for the ORFEO-NMGRID correlation 7-33
Table 7-15 Overall statistics of the combined data set for the ORFEO-NMGRID correlation 7-37
Table 7-16 Statistical parameters and design limit for ORFEO-NMGRID correlation 7-40
Table 7-17 Distribution of statepoints below the ORFEO-NMGRID correlation design limit by pressure ranges 7-41
Table 7-18 Distribution of statepoints below the ORFEO-NMGRID correlation design limit by mass flux ranges 7-42
Table 7-19 Distribution of statepoints below the ORFEO-NMGRID correlation design limit by equilibrium quality ranges 7-42
Table 7-20 Overall statistics of the combined data set for the ORFEO-NMGRID correlation by subchannel type 7-44
Table 7-21 Overall statistics of the combined data set for the ORFEO-NMGRID correlation by axial power profile type 7-44

Table 7-22 Results of statistical tests applied to ORFEO-NMGRID combined data set (subchannel and axial power profile type) 7-44

Table 7-23 Range of application for ORFEO-NMGRID CHF correlation (local thermal-hydraulic conditions) 7-53

Table B-1 Test assembly conditions for mixing grid tests ……..……..... B-1

Table B-2 Local conditions from COBRA-FLX simulations for mixing grid tests B-34

Table B-3 Test assembly conditions for non-mixing grid tests B-86

Table B-4 Local conditions from COBRA-FLX simulations for non-mixing grid tests ……..…… B-127

List of Figures

Figure 2-1 Correlations' application to GAIA fuel assembly 2-5
Figure 4-1 KATHY test loop 4-3
Figure 4-2 Monitoring of loop stability during CHF testing (pressure)..... 4-9
Figure 4-3 Radial geometry of the 5-by-5 test section – unit subchannel configuration (tests with prefix other than "SI") 4-11
Figure 4-4 Radial geometry of the 5-by-5 test section – guide tube subchannel configuration 4-12
Figure 4-5 Radial geometry of the 5-by-5 test section – unit subchannel configuration (tests with the prefix "SI")..... 4-13
Figure 4-6 Axial power profiles for the mixing grid tests 4-14
Figure 4-7 Axial power profiles for the non-mixing grid tests 4-15
Figure 6-1 CHF versus equilibrium quality 6-4
Figure 6-2 Definition of burnout length (Z_{BO}) 6-5
Figure 6-3 Definition of grid spacing and distance-to-grid 6-6
Figure 6-4 Distribution of the defining and validation data sets for the ORFEO-GAIA correlation (mass flux vs. pressure)..... 6-19
Figure 6-5 Distribution of the defining and validation data sets for the ORFEO-GAIA correlation (equilibrium quality vs. pressure) 6-20
Figure 6-6 Distribution of the defining and validation data sets for the ORFEO-GAIA correlation (equilibrium quality vs. mass flux) 6-21
Figure 6-7 Distribution of the defining and validation data sets for the ORFEO-NMGRID correlation (mass flux vs. pressure)..... 6-24
Figure 6-8 Distribution of the defining and validation data sets for the ORFEO-NMGRID correlation (equilibrium quality vs. pressure) 6-25
Figure 6-9 Distribution of the defining and validation data sets for the ORFEO-NMGRID correlation (equilibrium quality vs. mass flux) 6-26
Figure 6-10 Predicted CHF as a function of pressure for ORFEO-GAIA correlation ($gsp = dg = 0.521\ m$)..... 6-28
Figure 6-11 Predicted CHF as a function of mass flux for ORFEO-GAIA correlation ($gsp = dg = 0.521\ m$)..... 6-29
Figure 6-12 Predicted CHF as a function of effective quality for ORFEO-GAIA correlation ($gsp = dg = 0.521\ m$)..... 6-30
Figure 6-13 Predicted CHF as a function of pressure for ORFEO-NMGRID correlation ($gsp = dg = 0.521\ m$)..... 6-31

Figure 6-14 Predicted CHF as a function of mass flux for ORFEO-NMGRID correlation ($gsp = dg = 0.521\ m$) 6-32

Figure 6-15 Predicted CHF as a function of effective quality for ORFEO-NMGRID correlation ($gsp = dg = 0.521\ m$) 6-33

Figure 7-1 Histogram of the defining data set for the ORFEO-GAIA correlation 7-2

Figure 7-2 Histogram of the validation data set for the ORFEO-GAIA correlation 7-3

Figure 7-3 M/P versus pressure for ORFEO-GAIA correlation (defining and validation data sets) 7-5

Figure 7-4 M/P versus mass flux for ORFEO-GAIA correlation (defining and validation data sets) 7-6

Figure 7-5 M/P versus equilibrium quality for ORFEO-GAIA correlation (defining and validation data sets) 7-7

Figure 7-6 Histogram of the combined data set for the ORFEO-GAIA correlation 7-9

Figure 7-7 M/P versus pressure for the ORFEO-GAIA correlation for [ ] 7-16

Figure 7-8 M/P versus pressure for ORFEO-GAIA correlation (combined data set) 7-19

Figure 7-9 M/P versus mass flux for ORFEO-GAIA correlation (combined data set) 7-20

Figure 7-10 M/P versus equilibrium quality for ORFEO-GAIA correlation (combined data set) 7-21

Figure 7-11 M/P versus distance-to-grid for ORFEO-GAIA correlation (combined data set) 7-22

Figure 7-12 M/P versus grid spacing for ORFEO-GAIA correlation (combined data set) 7-23

Figure 7-13 M/P versus pressure for ORFEO-GAIA correlation [ ] 7-24

Figure 7-14 M/P versus mass flux for ORFEO-GAIA correlation [ ] 7-25

Figure 7-15 M/P versus equilibrium quality for ORFEO-GAIA correlation [ ] 7-26

Figure 7-16 M/P versus burnout length for ORFEO-GAIA correlation [ ] 7-27

Figure 7-17 Distribution of the combined data set [ ] for the ORFEO-GAIA correlation (mass flux vs. pressure) 7-29

Figure 7-18 Distribution of the combined data set [ ] for the ORFEO-GAIA correlation (equilibrium quality vs. pressure) 7-30

Figure 7-19 Distribution of the combined data set [ ] for the ORFEO-GAIA correlation (equilibrium quality vs. mass flux) 7-31

Figure 7-20 M/P versus pressure for ORFEO-NMGRID correlation (defining and validation data sets) 7-34

Figure 7-21 M/P versus mass flux for ORFEO-NMGRID correlation (defining and validation data sets) 7-35

Figure 7-22 M/P versus equilibrium quality for ORFEO-NMGRID correlation (defining and validation data sets) 7-36

Figure 7-23 Histogram of the combined data set for the ORFEO-NMGRID correlation 7-38

Figure 7-24 M/P versus pressure for ORFEO-NMGRID correlation (combined data set) 7-45

Figure 7-25 M/P versus mass flux for ORFEO-NMGRID correlation (combined data set) 7-46

Figure 7-26 M/P versus equilibrium quality for ORFEO-NMGRID correlation (combined data set) 7-47

Figure 7-27 M/P versus distance-to-grid for ORFEO-NMGRID correlation (combined data set) 7-48

Figure 7-28 M/P versus grid spacing for ORFEO-NMGRID correlation (combined data set) 7-49

Figure 7-29 Distribution of the combined data set for the ORFEO-NMGRID correlation (mass flux vs. pressure) 7-51

Figure 7-30 Distribution of the combined data set for the ORFEO-NMGRID correlation (equilibrium quality vs. pressure) 7-52

Figure 7-31 Distribution of the combined data set for the ORFEO-NMGRID correlation (equilibrium quality vs. mass flux) 7-53

Figure 7-32 M/P versus pressure for the mixing grid CHF data set evaluated with the ORFEO-NMGRID correlation 7-55

Figure 7-33 M/P versus mass flux for the mixing grid CHF data set evaluated with the ORFEO-NMGRID correlation 7-56

Figure 7-34 M/P versus equilibrium quality for the mixing grid CHF data set evaluated with the ORFEO-NMGRID correlation 7-57

Figure 8-1 GAIA structural grid - guide tube configurations 8-3

Figure 8-2 Depiction of various unit cell flap configurations 8-3
Figure 8-3 Vane slots on GAIA grid..... 8-4
Figure A-1 Axial geometry of CHF test K7100.....A-1
Figure A-2 Axial geometry of CHF test K7300.....A-2
Figure A-3 Axial geometry of CHF test K760x A-3
Figure A-4 Axial geometry of CHF test K770x A-4
Figure A-5 Axial geometry of CHF test K780x A-5
Figure A-6 Axial geometry of CHF test K8100.....A-6
Figure A-7 Axial geometry of CHF test K820x A-7
Figure A-8 Axial geometry of CHF test K830x A-8
Figure A-9 Axial geometry of CHF test K840x A-9
Figure A-10 Axial geometry of CHF test K8601.....A-10
Figure A-11 Axial geometry of CHF test AR6.....A-11
Figure A-12 Axial geometry of CHF test AR7.....A-12
Figure A-13 Axial geometry of CHF test AR8.....A-13
Figure A-14 Axial geometry of CHF test AR9.....A-14
Figure A-15 Axial geometry of CHF test AR11.....A-15
Figure A-16 Axial geometry of CHF test AR12.....A-16
Figure A-17 Axial geometry of CHF test K6800.....A-17
Figure A-18 Axial geometry of CHF test K8500.....A-18
Figure A-19 Axial geometry of CHF test O1500.....A-19
Figure A-20 Axial geometry of CHF test SI110/SI111.....A-20
Figure A-21 Axial geometry of CHF test SI190.....A-21
Figure A-22 Axial geometry of CHF test SI210.....A-22
Figure A-23 Axial geometry of CHF test SI340.....A-23
Figure C-1 Flow chart of the genetic algorithm C-5
Figure C-2 Three stage correlation fitting process C-6

Nomenclature

Acronym	Definition
AFA-3G	AFA-3G grid design
AOO	Anticipated Operational Occurrence
ARC	Alliance Research Center
BOHL	Beginning of Heated Length
BWR	Boiling Water Reactor
CEA	French Atomic Energy Commission (*Commissariat à l'énergie atomique*)
CHF	Critical Heat Flux
DNB	Departure from Nucleate Boiling
DNBR	Departure from Nucleate Boiling Ratio
EOHL	End of Heated Length
GAIA	AREVA's PWR fuel assembly and grid design
GDC	General Design Criterion
HMP	HMP grid design
HTP	HTP grid design
HTRF	Columbia University's Heat Transfer Research Facility
IGM	Intermediate GAIA Mixer
KATHY	Karlstein Thermal-Hydraulic test facility
M/P	Measured CHF divided by predicted CHF
MDNBR	Minimum Departure from Nucleate Boiling Ratio
NMGRID	Non-mixing grid design
NRC	U.S. Nuclear Regulatory Commission
OD	Outer diameter
ORFEO	AREVA's CHF correlation form for PWR fuel assemblies
PWR	Pressurized Water Reactor
SER	Safety Evaluation Report
SRP	U.S. NRC Standard Review Plan
SSG	Simple Support Grid
TC	Thermocouple

ABSTRACT

A fuel assembly design for pressurized water reactors, called GAIA, has been developed by AREVA. The GAIA fuel assembly is equipped with structural grids (GAIA) and may optionally include mid-span-mixing grids, called intermediate GAIA mixers (IGMs). The GAIA and IGM grids have mixing devices (vanes). The lower end grid and the upper end grid are HMP grids, which do not have mixing devices.

This report documents two critical heat flux correlations. The first is a mixing grid correlation based on the CHF tests performed for grids with mixing vanes (GAIA structural grid and IGM grid). This correlation is referred to as ORFEO-GAIA; it is applicable to fuel assemblies that are equipped with GAIA grids, with or without IGM grids. The second is a non-mixing grid correlation based on the CHF tests performed for [ ] without mixing devices. This correlation is referred to as ORFEO-NMGRID; it is applicable to fuel assemblies equipped with [ ] This report describes the correlations' development, data sets, and resulting application design limits and applicability ranges.

1.0 INTRODUCTION

AREVA has developed a fuel assembly design for pressurized water reactors, called GAIA. The GAIA fuel assembly is equipped with structural grids (GAIA) and may optionally include mid-span-mixing grids, called intermediate GAIA mixers (IGMs). The lower end grid and the upper end grid are HMP grids. The GAIA structural grid is developed specifically for the GAIA fuel assembly. It features two improvements to proven technologies: [

] The IGM grid is an evolutionary design based on the AFA-3G grid design. AFA-3G grids are widely used on AREVA fuel assemblies supplied to European customers. The IGM has mixing vanes for increased CHF performance. The HMP grid for the GAIA fuel assembly is based on the existing HMP grid design, which is used on AREVA fuel assemblies supplied to U.S. and European customers. The HMP grid features a linear fuel rod contact similar in concept to the structural grids and has no mixing vanes. The structure of the GAIA fuel assembly including IGMs is illustrated in Figure 2-1. Correlations are needed to describe the CHF performance of the GAIA fuel assembly.

This report describes the development and validation of two CHF correlations:

- A mixing grid correlation based on the CHF tests performed for grids with mixing vanes (GAIA structural grid and IGM grid). This correlation is referred to as ORFEO-GAIA.
- A non-mixing grid correlation based on the CHF tests performed for several different grid designs without mixing devices. This correlation is referred to as ORFEO-NMGRID.

The CHF correlations described in this report use a correlation form based on a modular approach that separates the general critical heat flux parameters from the fuel design specific parameters. This correlation form is referred to as ORFEO.

Section 2.0 of this report summarizes the statistical analysis and the applicability ranges for the two CHF correlations. Section 3.0 identifies the applicable regulatory requirements. Section 4.0 describes the CHF testing program. Section 5.0 discusses the code used for thermal-hydraulic simulations. Section 6.0 describes the development of the generic ORFEO correlation and the specific grid parameters for the ORFEO-GAIA and the ORFEO-NMGRID correlations. Section 7.0 describes the statistical analysis performed based on the measured-to-predicted (M/P) CHF ratios, the calculation of the design limit and the determination of the application range for each of the two correlations. Section 8.0 compares the features of the CHF test assembly to those of the production assembly. Section 9.0 describes the quality assurance program applicable to the CHF testing and CHF correlations' development and validation.

AREVA is requesting approval for the following:

- the ORFEO-GAIA CHF correlation (Section 2.1) applied to fuel assemblies equipped with GAIA grids, with and without IGMs, as described in Section 2.3
- the ORFEO-NMGRID CHF correlation (Section 2.2) applied to fuel assemblies equipped with GAIA grids, with and without IGMs, and bottom HMP grid, as described in Section 2.3

2.0 SUMMARY

2.1 *ORFEO-GAIA CHF correlation*

Key statistical parameters of the ORFEO-GAIA CHF correlation are provided in Table 2-1. The ORFEO-GAIA CHF correlation is applicable to fuel assemblies equipped with GAIA grids, with or without IGM grids. The range of applicability is provided in Table 2-2 (local thermal-hydraulic conditions) and Table 2-3 (fuel assembly geometry). The ORFEO-GAIA CHF correlation is applicable with the subchannel thermal-hydraulic analysis code COBRA-FLX.

Table 2-1 Key statistical parameters of the ORFEO-GAIA correlation

Parameter	Value
Design limit	1.11
Mean of the M/P population	[ ]
Standard deviation of the M/P population	[ ]

Table 2-2 Range of application for ORFEO-GAIA correlation (local thermal-hydraulic conditions)

Parameter	Units	Minimum value	Maximum value
Pressure	MPa	9.97	17.45
	psia	1446.0	2530.9
Mass flux	kg/m^2s	679.8	4323.4
	Mlb_m/ft^2hr	0.5012	3.1878
Equilibrium quality	fraction	---	0.7992

Table 2-3 Geometry for ORFEO-GAIA correlation (fuel assembly geometry)

2.2 *ORFEO-NMGRID CHF correlation*

Key statistical parameters of the ORFEO-NMGRID CHF correlation are provided in Table 2-4. The ORFEO-NMGRID CHF correlation is applicable to fuel assemblies equipped with non-mixing grids. The range of applicability is provided in Table 2-5 (local thermal-hydraulic conditions) and Table 2-6 (fuel assembly geometry). The ORFEO-NMGRID CHF correlation is applicable with the subchannel thermal-hydraulic analysis code COBRA-FLX.

Table 2-4 Key statistical parameters of the ORFEO-NMGRID correlation

Parameter	Value
Design limit	1.15
Mean of the M/P population	[ ]
Standard deviation of the M/P population	[ ]

Table 2-5 Range of application for ORFEO-NMGRID correlation (local thermal-hydraulic conditions)

Parameter	Units	Minimum value	Maximum value
Pressure	MPa	2.01	17.46
	psia	291.5	2532.4
Mass flux	kg/m^2s	406.5	4826.0
	Mlb_m/ft^2hr	0.2997	3.5584
Equilibrium quality	fraction	---	0.8769

Table 2-6 Geometry for ORFEO-NMGRID correlation (fuel assembly geometry)

[ ]

2.3 *Correlations' application to the GAIA fuel assembly*

The ORFEO-GAIA and ORFEO-NMGRID CHF correlations' application to the GAIA fuel assembly is illustrated in Figure 2-1. They are applicable to GAIA fuel assemblies with or without IGMs.

The non-mixing grid region is between the beginning of heated length (BOHL) and the top plane of the first mixing grid. The mixing grid region is between the top plane of the first mixing grid and the end of heated length (EOHL).

For the mixing grid region of the GAIA fuel assembly the following correlations are applicable:

[ ]

For the non-mixing grid region of the GAIA fuel assembly [

]

Figure 2-1 Correlations' application to GAIA fuel assembly

3.0 REGULATORY REQUIREMENTS APPLICABLE TO THIS REPORT

Steady state and transient codes and methods used for licensing basis analyses are subject to regulatory requirements and guidance specified in the Standard Review Plan (SRP) (NUREG-0800) [1]. SRP Section 4.4, “Thermal and Hydraulic Design” provides criteria acceptable to meet the relevant requirements of General Design Criterion (GDC) 10 of 10 CFR Part 50, Appendix A. GDC 10 requires that “the reactor core and associated coolant, control, and protection systems shall be designed with appropriate margin to assure that specified acceptable fuel design limits are not exceeded during any condition of normal operation, including the effects of anticipated operational occurrences.” Acceptance Criterion 1.A. of SRP Section 4.4 states that for correlations used to predict critical heat flux, there should be a 95% probability at the 95% confidence level that the hot rod in the core does not experience a DNB or boiling transition condition during normal operation or Anticipated Operational Occurrences (AOOs). The correlations and associated design limits in this report meet this criterion when used within the specified ranges of applicability.

4.0 CHF TESTING AND DATA

4.1 *CHF test facilities*

The phenomenon of CHF cannot be predicted from first principles; therefore, it is measured under laboratory conditions approximating those of a real reactor core. A CHF correlation is developed based on these experimental measurements.

For PWR fuel assemblies, the CHF performance is measured by testing full length sections of the fuel assembly under reactor conditions. Electrically heated rods simulate the nuclear heating of fuel rods. The power of the test assembly is slowly increased until the boiling crisis is detected via a sudden increase in temperature. The critical power of the test assembly is measured as a function of system pressure, inlet mass flux and inlet temperature (subcooling). Depending on the local thermal-hydraulic conditions, both departure from nucleate boiling (DNB) and dryout phenomena can be observed.

The CHF tests (experiments) are conducted in test loops – complex thermo-fluid systems capable of simulating the reactor core thermal-hydraulic conditions. The CHF testing programs for the two CHF correlations developed and verified in this report use tests performed in four loops, as described below.

The CHF tests identified with the prefix “K” in this report were performed in the KATHY loop – AREVA’s test facility located in Karlstein, Germany. The KATHY loop is illustrated in Figure 4-1. Since 1986, it has been extensively used to collect test data for licensing of PWR and BWR fuel assemblies.

Tests performed at the Babcock and Wilcox’s Alliance Research Center (ARC) test facility are identified with the prefix “AR”. These tests supported the NRC-approved BWC and BWU-N CHF correlations in [2] and [3], respectively.

Tests performed at the Columbia University's Heat Transfer Research Facility (HTRF) are identified with the prefix "SI". This facility has been extensively used as a source of CHF test data for correlations approved by the U.S. NRC (e.g., BWU-Z and BHTP approved in [3] and [4], respectively).

The test performed at CEA's OMEGA loop located in Grenoble, France is identified with the prefix "O".

The qualification of KATHY as an acceptable source of CHF test data for CHF correlation development was provided with the ACH-2 CHF correlation in Section 2.2 of [5]. Additional benchmarking of the KATHY, OMEGA and HTRF test loops is provided in [6], where CHF measurements obtained from these test facilities were evaluated with an applicable CHF correlation and compared in terms of mean and standard deviation of the M/P population (Table 4-1). The benchmark validates the CHF test results obtained at each of these facilities.

Table 4-1 Overall statistic results for test facilities benchmark

Test	KATHY	OMEGA	HTRF	ALL DATA
Mean	1.028	1.030	1.037	1.032
Standard deviation	0.051	0.048	0.069	0.056
Number of statepoints	44	44	44	132

Figure 4-1 KATHY test loop

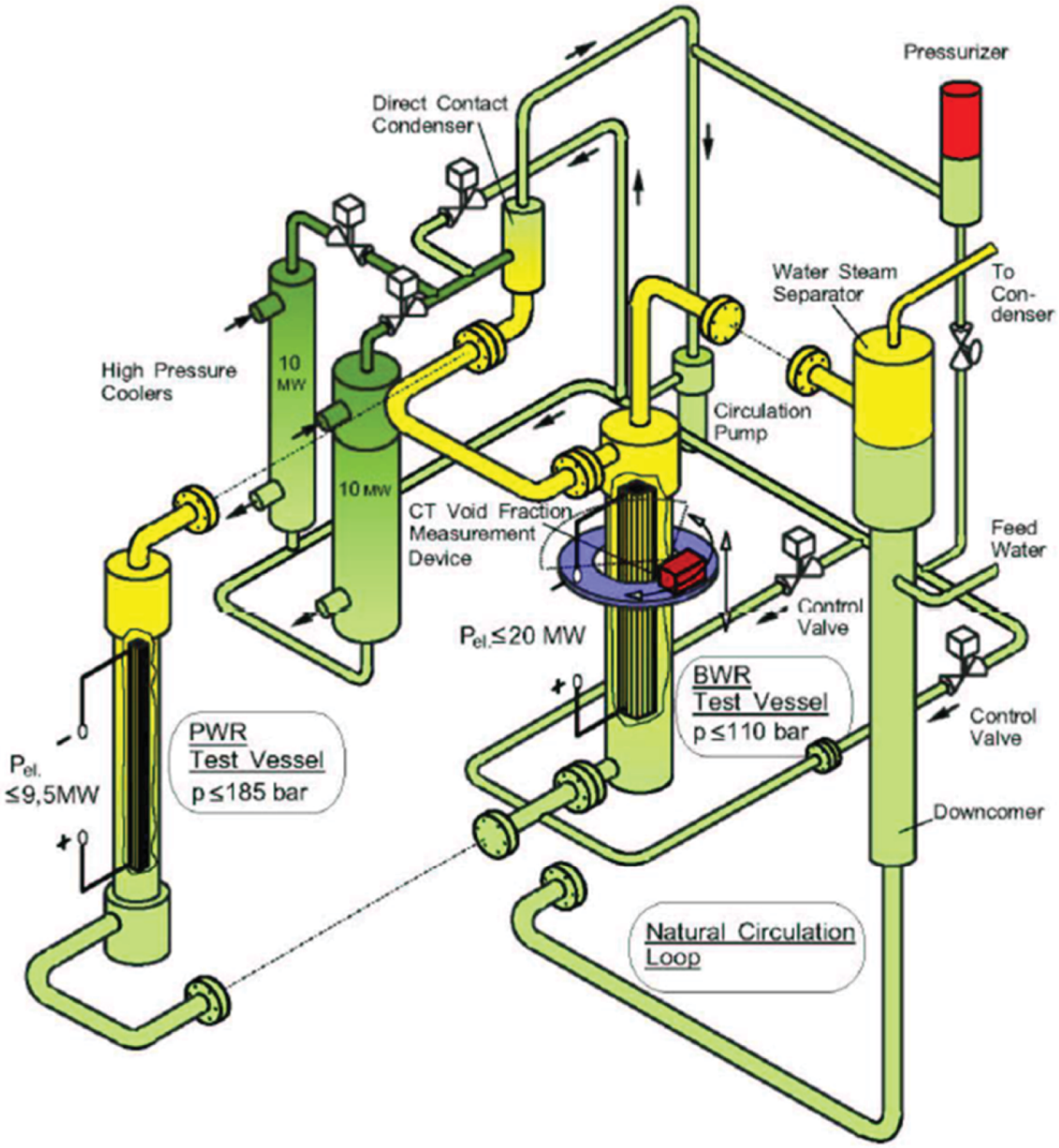

KATHY loop characteristics

The test vessel is designed to a maximum pressure of 185 bar (2683 psia) and a maximum fluid temperature of 360 °C (680 °F). The 300 kW pressurizer has a volume of one cubic meter and a design pressure and temperature consistent with the test vessel. The circulation pump has a design maximum pressure of 210 bar (3046 psia) and a design maximum temperature of 370 °C (698 °F). The loop's electrical power supply has a maximum (gross) power of approximately 20 MWe and a maximum current of 80 kA at 230 V DC.

KATHY loop instrumentation

The inlet temperature is measured at the test vessel inlet by two independent, calibrated temperature sensors. The outlet temperature is measured by three temperature sensors. The absolute system pressure is measured by two pressure transducers at the outlet of the test section (flow channel). Two independent and diverse methods are applied to measure the electric current to the test assembly: the first is based on the Faraday effect and the second is based on four high precision fast response shunts. At least one heater rod is equipped with voltage taps across the heated length. This measurement is used to determine the electric power to the test assembly. As a backup, the voltage between the busbars is measured. The mass flow rate is measured using two orifices and the pressure drop across the orifices is measured using pressure transducers. [

]

Table 4-2 lists the uncertainties of electrical power, system pressure, inlet temperature and mass flow in the KATHY loop. Based on these individual components, [

]

Table 4-2 KATHY test loop uncertainties

Measurement	Uncertainty
Electrical power	[ ]
System pressure	[ ]
Inlet temperature	[ ]
Mass flow	[ ]

The heat loss of the KATHY loop test vessel for PWR tests was evaluated and found to be [ ] The heat loss is the fraction of heat generated in the test assembly that does not contribute to the enthalpy increase of the fluid flowing through the test section (i.e., is lost through the test channel walls).

All CHF tests used direct heater rods. A direct heater rod consists of a metal tube (usually Inconel) equipped with thermocouples. These are placed on the inner wall of the tube using ceramic pieces to ensure electric insulation. Heat is generated by passing an electric current through the heater rod wall (Ohmic heating). An axial power profile is created by varying the thickness of the wall. The outer diameter is constant and fixed. The inner diameter is varied resulting in a wall thickness profile that creates the desired axial power profile. Thermocouples are placed at multiple axial elevations in order to detect the occurrence of CHF and also to protect the integrity of the test assembly. The thermocouples are placed in the locations where CHF (or dryout) is expected to occur. The CHF is detected by a sudden increase in the temperature indicated by one or more thermocouples.

KATHY loop data acquisition system

The analog signals of the loop instrumentation are sampled by digital converter and stored on hard disk. Analog and digital input channels are available. The sample rate per channel is 20 Hz. Six computers monitor the test. One computer controls the acquisition and flow of data. Three computers display and visualize selected channels, especially the thermocouples during CHF tests. One computer displays the test results immediately after a statepoint is measured. The sixth computer is used to access the CHF test data. The evaluation software is used to transfer the measured values (voltages) into physical values (e.g., pressure, temperature and mass flow).

4.2 *CHF test program*

4.2.1 Test procedure and data collection methods

This section describes the test procedure and data collection methods for the new data supporting this report, obtained from the KATHY test loop.

Each measured CHF statepoint is described by nominal values of pressure, mass flux and inlet temperature prescribed in the test requirements document. The pressure is set and then the inlet flow rate and the inlet temperature are set. When the loop is observed to be steady at the boundary conditions specified for the measurement, the power is slowly increased until CHF is detected. [ ] used to check for the occurrence of onset of CHF: [ ] For the next statepoint, the inlet flow rate is increased or decreased and the process is repeated. Typically, when all of the measurements at one inlet temperature are completed, the inlet temperature is changed. When all of the measurements at one pressure are completed, the pressure is increased or decreased and the process is repeated.

Because the CHF test results are ordered, most abnormalities in the test are immediately evident. When the pressure and inlet flow are set, the critical power will vary linearly with the inlet temperature. The slope of the line increases as the inlet flow increases.

When performing CHF testing, the loop stability is controlled by monitoring the pressure, inlet flow and inlet temperature. The nominal values for pressure, mass flux and inlet temperature that characterize each CHF statepoint are prescribed. In order to ensure that the CHF test data is collected as intended, the values set for pressure, inlet flow and inlet temperature are not allowed to deviate from the nominal values beyond the ranges specified in Table 4-3.

In order to ensure stability of the local thermal-hydraulic parameters during CHF measurements, the following restrictions are imposed for pressure, inlet flow and inlet temperature:

If outside of these ranges, the measurement is repeated. Figure 4-2 provides a visual description of how the loop stability is controlled when performing CHF testing. This particular example is for the system pressure. The chart is based on the information in Table 4-3, Table 4-4 and Table 4-5.

Table 4-3 Maximum deviations of CHF test parameters from nominal values

Parameter	Maximum deviation from nominal value
Pressure	[ ]
Inlet mass flux	[ ]
Inlet temperature	[ ]

Table 4-4 Maximum deviations of CHF test parameters from [ ]

Parameter	Maximum deviation from [ ]
Pressure	[ ]
Inlet mass flux	[ ]
Inlet temperature	[ ]

Table 4-5 Maximum deviations of CHF test parameters from [ ]

Parameter	Maximum deviation from [ ]
Pressure	[ ]
Inlet mass flux	[ ]
Inlet temperature	[ ]

Figure 4-2 Monitoring of loop stability during CHF testing (pressure)

A reference statepoint is defined for the purpose of checking the integrity of the test assembly during the progress of the testing. This reference point is characterized by a specific prescribed pressure, flow rate and inlet temperature. [

]

Upon completion of the CHF testing, the test assembly is inspected. [

] are measured and recorded in order to establish the validity of the CHF test data collected. The heater rods are inspected for [

]

4.2.2 Test assembly configurations

All CHF tests (Table 4-8 and Table 4-9) were performed in a 5-by-5 rod configuration, which is the standard practice for PWR CHF testing. Two configurations are tested: *(i)* a unit subchannel and *(ii)* a guide tube subchannel. Each unit subchannel test assembly has 25 heater rods simulating the fuel rods (Figure 4-3 and Figure 4-5). Each guide tube subchannel test assembly has 24 heater rods and an unheated rod located at the center of the matrix, simulating the guide tube (Figure 4-4). A unit subchannel is defined to be a channel that is adjacent to 4 heater rods. A guide tube subchannel is defined to be a channel that is adjacent to 3 heater rods and 1 guide tube. Table 4-8 and Table 4-9 list the geometry parameters for the mixing and non-mixing grid tests, respectively. The axial position of the grids are shown in Appendix A. The non-uniform axial power profiles for the mixing and non-mixing grid tests are shown in Figure 4-6 and Figure 4-7, respectively. The radial peaking factors for the mixing and non-mixing grid tests are shown in Table 4-6 and Table 4-7, respectively. Note that the rod numbering system for the CHF tests with the prefix “SI” is different from the other tests (Figure 4-5).

The power of the central heater rods is higher than the power of the peripheral heater rods by approximately 10% to 20% (Figure 4-3, Figure 4-4 and Figure 4-5) in order to assure that the radial location of CHF is away from the periphery of the test assembly. This reduces the test channel wall impact on the flow field at the location of the CHF.

In an electrically heated test assembly with direct heater rods, electromagnetic forces are created. Therefore, it was necessary to strengthen the test assembly in order to ensure prototypic geometry was preserved under test conditions. For some test assemblies, the strengthening was achieved by (*i*) including simple support grids and (*ii*) placing motion limiters on the springs. The impact of these modifications on CHF measurements is negligible.

Figure 4-3 Radial geometry of the 5-by-5 test section – unit subchannel configuration (tests with prefix other than "SI")

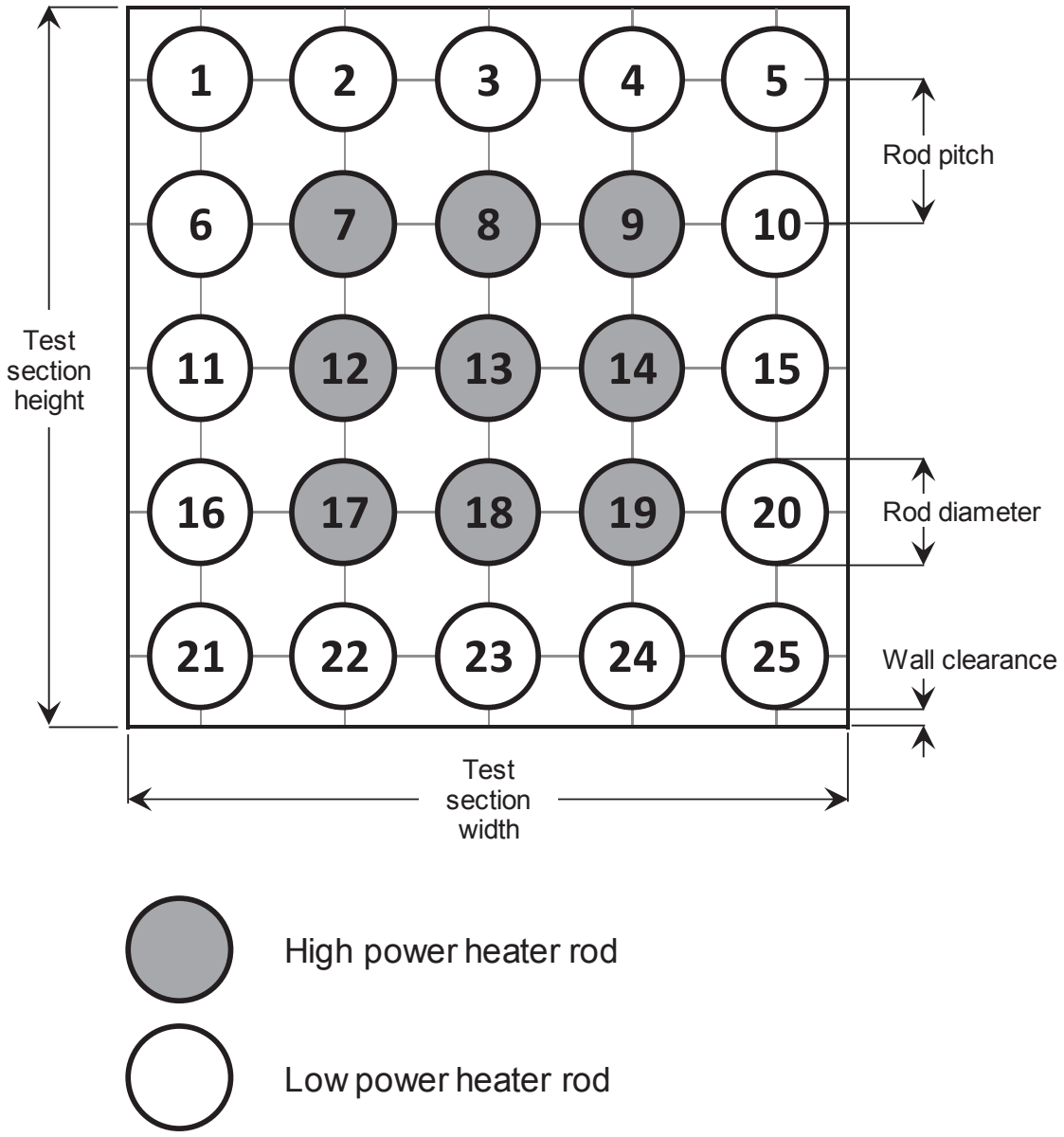

Figure 4-4 Radial geometry of the 5-by-5 test section – guide tube subchannel configuration

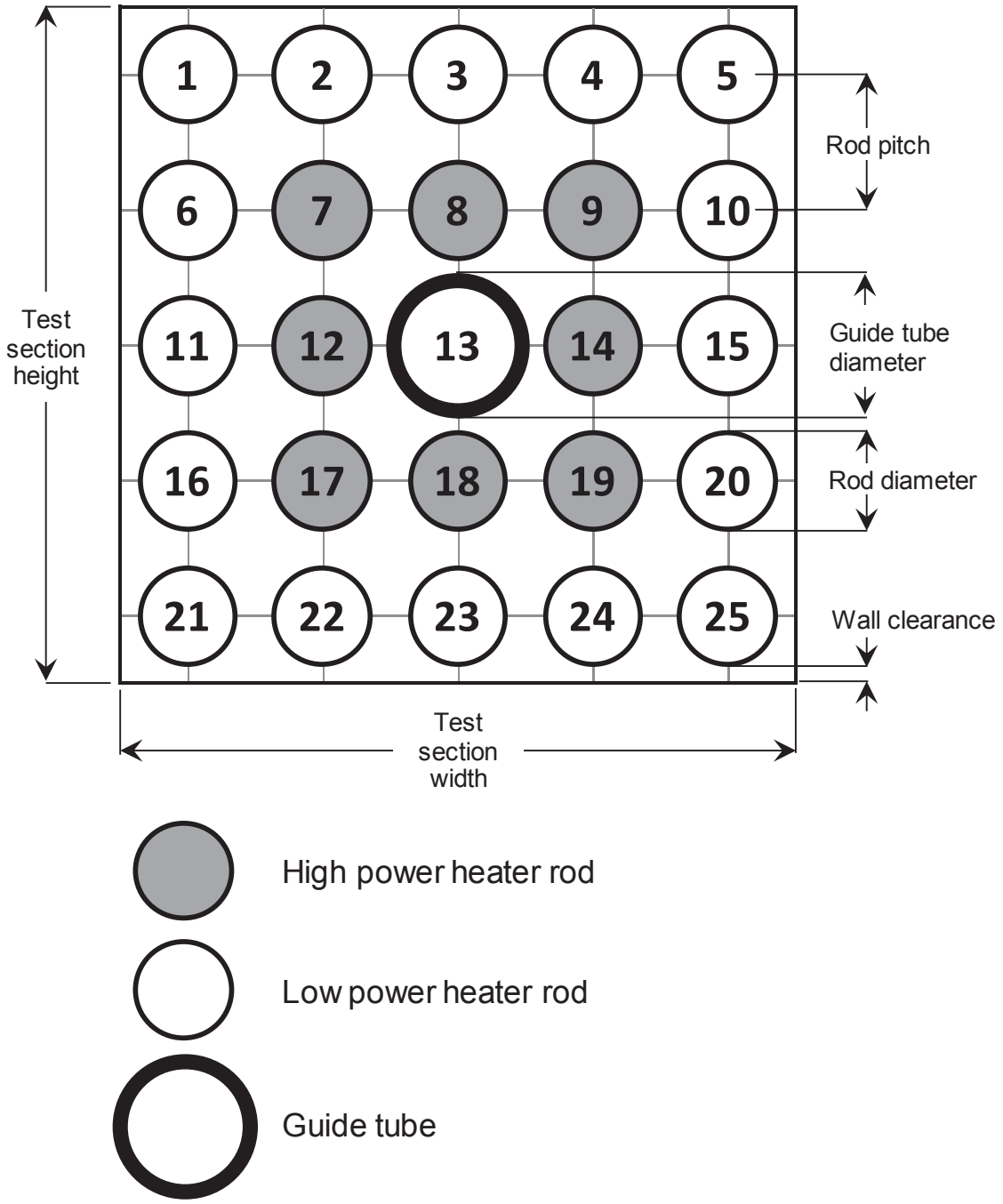

Figure 4-5 Radial geometry of the 5-by-5 test section – unit subchannel configuration (tests with the prefix "SI")

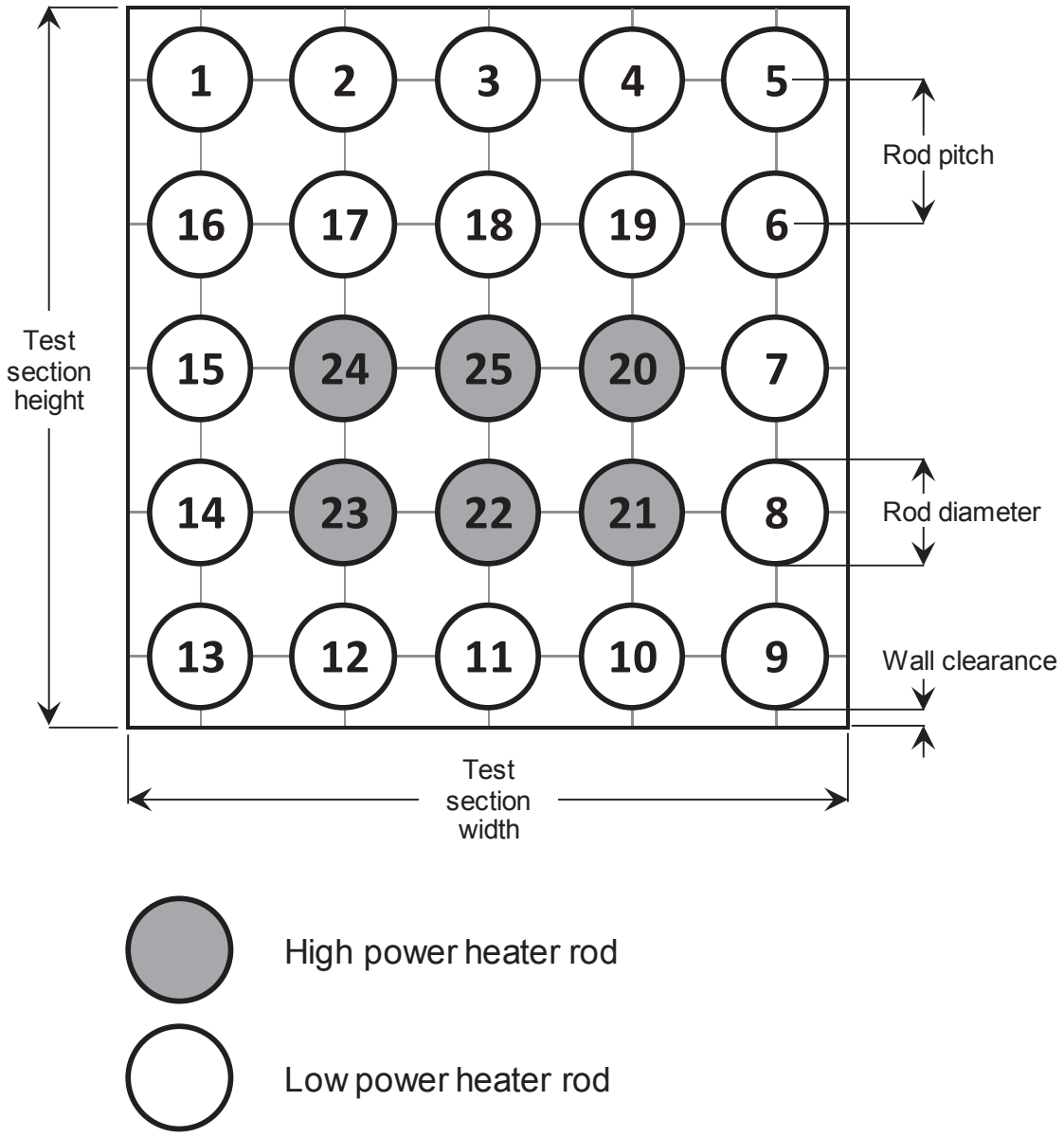

Figure 4-6 Axial power profiles for the mixing grid tests

Figure 4-7 Axial power profiles for the non-mixing grid tests

Table 4-6 Radial power factors for the mixing grid tests

Table 4-6 Radial power factors for the mixing grid tests (cont'd)

Table 4-7 Radial power factors for the non-mixing grid tests

Table 4-7 Radial power factors for the non-mixing grid tests (cont'd)

4.2.3 CHF test program design – mixing grid

The CHF test matrix supporting the ORFEO-GAIA CHF correlation is shown in Table 4-8. The matrix of individual tests provides a total of ten, one-parameter-at-a-time changes:

Note that in the bulleted list above a series of tests with the same configuration is indicated by an “x” (e.g., K7600 and K7601 are abbreviated as K760x).

The paired tests listed above allow the determination of the sensitivity of separate effects, which are accounted for in the ORFEO-GAIA CHF correlation.

Table 4-8 Mixing grid CHF tests

4.2.4 CHF test program design – non-mixing grid

The CHF test matrix supporting the ORFEO-NMGRID CHF correlation is shown in Table 4-9. Test K8500 features [

] The data set covers [

] Their common feature is [

]

Table 4-9 Non-mixing grid CHF tests

4.2.5 Data collection ranges

The development of a CHF correlation requires the acquisition of a data set that covers the application domain with a sufficient data density with an acceptable uncertainty. Pressure, mass flux and inlet temperature (subcooling) were all considered in developing the testing strategy to ensure that the application domain is adequately covered. An expanded coverage of the application domain in quality was achieved by collecting CHF statepoints characterized by a combination of high pressure and low inlet subcooling. This leads to local conditions characterized by high equilibrium quality (Figure 6-5 and Figure 6-8). CHF statepoints characterized by low pressure were measured for the mixing grid in order to demonstrate correlation applicability in this range.

4.3 *CHF test data*

Table B-1 contains the assembly conditions for the CHF statepoints that constitute the data set of the ORFEO-GAIA correlation.

Table B-2 contains the calculated local conditions for the CHF statepoints that constitute the data set of the ORFEO-GAIA correlation.

Table B-3 contains the assembly conditions for the CHF statepoints that constitute the data set of the ORFEO-NMGRID correlation.

Table B-4 contains the calculated local conditions for the CHF statepoints that constitute the data set of the ORFEO-NMGRID correlation.

5.0 SUBCHANNEL CODE

The PWR CHF correlations are developed based on local thermal-hydraulic conditions. The local thermal-hydraulic conditions are calculated by a subchannel code. The ORFEO-GAIA and ORFEO-NMGRID correlations are developed and verified using the subchannel code COBRA-FLX, which has been reviewed and approved by the U.S. NRC for application to nuclear core thermal-hydraulic analysis for steady-state and transient conditions in [7]. The subchannel code modeling requirements used for developing the ORFEO-GAIA and ORFEO-NMGRID correlations with COBRA-FLX are established based on the empirical correlations and numerical solution methods approved by the U.S. NRC in the SER issued for the COBRA-FLX Topical Report [7] and listed in Table 5-1.

Table 5-1 Empirical correlations and numerical solution methods used in the COBRA-FLX subchannel code model

Parameter	Value
Conservation equations	SCHEME-Pressure
Water properties	IAPWS-IF97
Subcooled void correlation	Saha-Zuber
Bulk void correlation	Chexal-Lellouche using the full curve fit routine
Two-phase friction multiplier	Homogeneous model
Wall friction factor	Standard model[1]
Wall friction correction	Wall viscosity correction included in the wall friction factor
Subcooled boiling profile fit	Zuber-Staub
Turbulent mixing coefficient[2]	[ ] for the mixing grids [ ] for the non-mixing grids
Diversion crossflow resistance	0.15
Turbulent momentum factor	1.0
Transverse momentum parameter	0.25

Notes:

1. [

]

2. The mixing behavior of the spacer grids is modelled via diffusion of energy (turbulent enthalpy exchange without mass exchange) across the gaps between subchannels. The turbulent mixing coefficients are determined from mixing tests performed with the CHF test assemblies. Thermocouples are attached at the exit of the test assembly and the subchannel temperature distribution is measured in single phase flow. The mixing coefficient is the value that minimizes the difference between measured temperatures and COBRA-FLX predicted temperatures.

6.0 CORRELATION DEVELOPMENT

6.1 *Background*

In PWR cores, energy is generated by uranium dioxide fuel pellets enclosed in fuel rods. The energy leaves the fuel rod surface in the form of heat flux, which is removed by the coolant system flow. The normal mode of heat transfer to the coolant at high power densities is nucleate boiling. Nucleate boiling is an efficient mode of heat transfer, with heat transfer coefficients about 280,000 W/m^2K.

As the capacity of the coolant to accept heat from the fuel rod surface and transfer it by bubble detachment to the coolant stream degrades, a continuous layer or film of steam starts to blanket the rod. The steam film insulates the rod and the heat transfer coefficient drops drastically to around 2800 W/m^2K. This is because the heat transfer mechanism is film boiling, primarily conduction through the steam layer.

Reactor cores must be protected against possible damage that could result from the high clad temperatures that are experienced in the transition to, and during, film boiling. The heat flux at which the steam film starts to form is termed the critical heat flux or the point of departure from nucleate boiling (DNB).

For design purposes, the departure from nucleate boiling ratio (DNBR) is used as an indicator of the margin to DNB. The DNBR is the ratio of the predicted CHF to the actual heat flux at the same condition. Therefore, the DNBR is a measure of the thermal margin to film boiling and its associated high temperatures. In general, a higher DNBR value leads to a higher thermal margin.

The CHF cannot be predicted from first principles, so it is empirically correlated as a function of the local thermal-hydraulic conditions, the geometry and the power distribution measured in experiments. CHF test data are typically obtained from experiments under steady state conditions. It is common practice, based on experimental evidence, to assume the CHF, during a transient situation, will be exceeded when the local instantaneous conditions are equivalent to those causing its occurrence under steady-state conditions, as discussed in Section 9.6.2 of [8]. Because a CHF correlation is essentially a surface fit to experimental data, it has an associated uncertainty. This uncertainty is quantified in a DNBR design limit, consistent with the specified acceptable fuel design limit discussed in [1]. A calculated DNBR value greater than this design limit ensures that there is, at a minimum, a 95% probability with 95% confidence (95/95) that a departure from nucleate boiling will not occur. [

]

AREVA has developed and continues to use numerous CHF correlations for its fuel assemblies. The two most recently reviewed and approved by the U.S. NRC are the BHTP correlation [4] and the ACH-2 correlation [5]. The two CHF correlations described in this report are based on a different mathematical form, called ORFEO; they exhibit many similarities with previously licensed correlations (e.g., [4] and [5]) in terms of the nature of dependent variables. The ORFEO correlation form, however, introduces improvements to reduce variability of the measured-to-predicted CHF ratio.

6.2 *ORFEO CHF correlation form*

The ORFEO CHF correlation utilizes a modular approach that separates the general representation parameters from the grid specific parameters. This approach is similar to the generalized subchannel CHF correlation for PWR and BWR fuel assemblies presented in [9] and the introduction of correction factors to extend the Groeneveld CHF tables in [10] to rod bundle geometries [11].

An experimental CHF data set based on various test configurations and local thermal-hydraulic conditions was used to identify the parameters that have impact on measured CHF:

- Local flow conditions: pressure, mass flux, equilibrium quality
- Test configurations: grid spacing, distance-to-grid, guide tube presence, axial power profile, hydraulic diameter / equivalent heated diameter

This is consistent with dependencies identified for previously licensed CHF correlations.

Local flow conditions

The equilibrium quality has a significant impact on the CHF and, at the same time, it has a complex behavior. In the ORFEO correlation form, the equilibrium quality dependence is described using a linear function at low qualities and an exponential function at high qualities. These two regions are connected using a quadratic function as illustrated in Figure 6-1.

Figure 6-1 CHF versus equilibrium quality

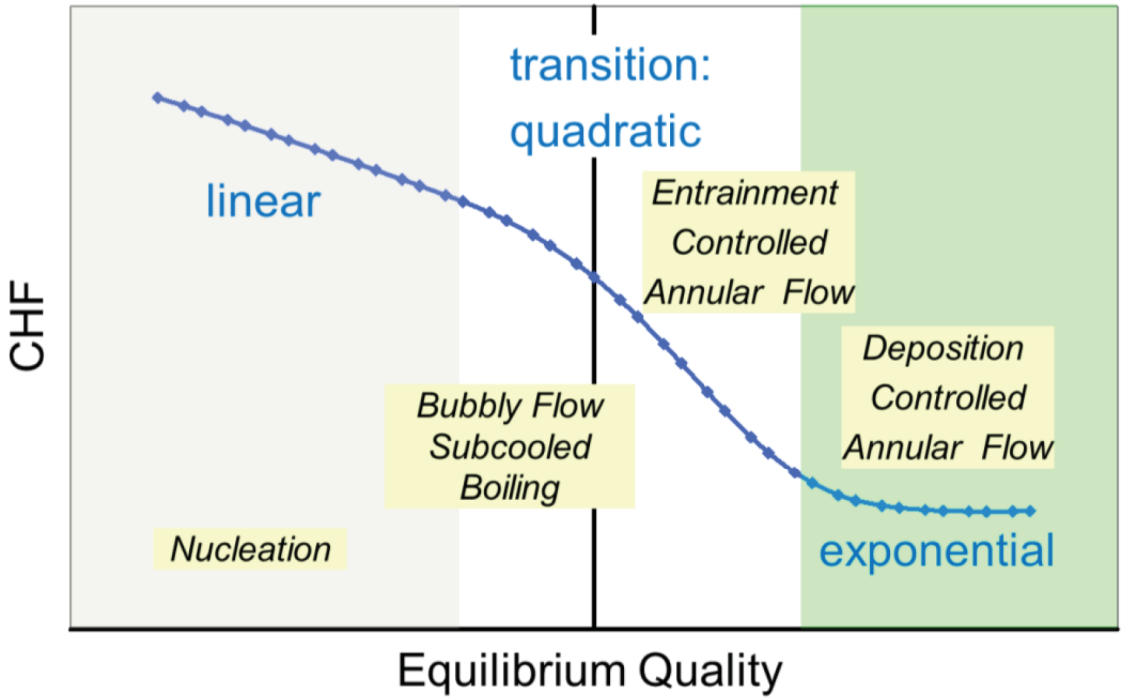

The ORFEO correlation form uses a parameter called "burnout length" (Z_{BO}). It is defined as the distance from the elevation where the equilibrium quality [ ] is reached to the elevation where CHF is calculated (Figure 6-2). The introduction of the burnout length parameter is a new feature, specific to the ORFEO CHF correlation form. It is similar to the boiling length present in some BWR critical power correlations. The burnout length is used to define how quality is incorporated into the correlation: [ ] An exponential damping factor is introduced to ensure a smooth transition between [ ]

Figure 6-2 Definition of burnout length (Z_{BO})

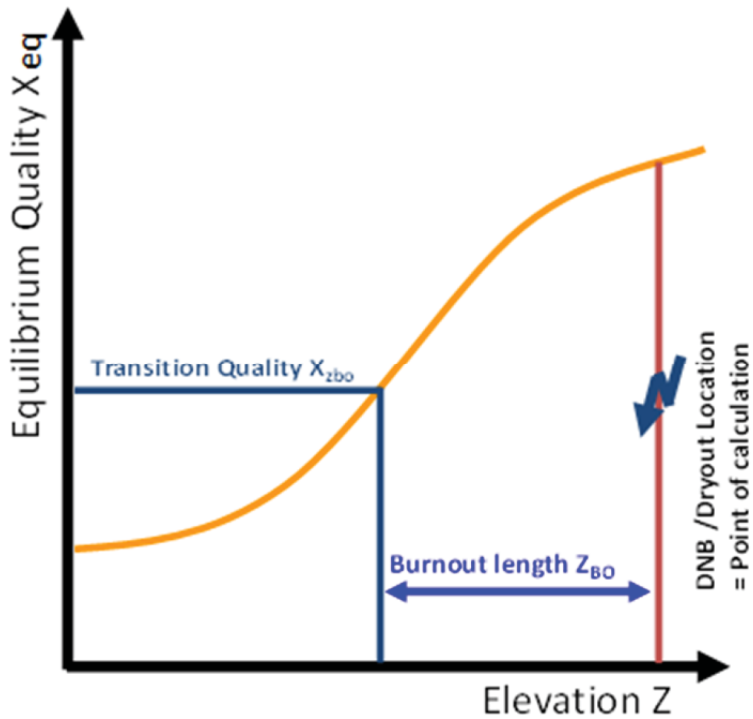

Grid spacing and distance-to-grid

Mixing vanes on grids improve the heat transfer from the rods by promoting fluid turbulence thereby, increasing the CHF performance. The level of turbulence downstream of a grid decreases gradually with the distance. In general, a shorter distance between two consecutive grids increases the CHF performance of a fuel assembly. This behavior is generally captured in empirical CHF correlations using two parameters:

- Grid spacing (gsp) – the distance between two consecutive grids
- Distance-to-grid (dg) – the distance between the CHF location and the upstream grid

In the ORFEO correlation form, the grid spacing dependence is implemented using [ ] This is based on the fact that the CHF performance at an axial location is not affected by [ ]

Figure 6-3 Definition of grid spacing and distance-to-grid

[ ]

Guide tube impact

The guide tube impact accounts for the difference in CHF performance between the unit subchannel and the guide tube subchannel. [ ]

Axial power profile

The impact of non-uniform axial power profiles is implemented using the axial power factor (FNU) based on the TONG factor method [12, Chapter 5.3.2.1]. The coefficients of the empirical factor K are adjusted to capture the effect of non-uniform axial power profiles using [ ] It should be noted that there is a close connection between [ ] used in the ORFEO correlation. [ ] represent a "memory" effect on the enthalpy distribution within each subchannel. Essentially, the average subchannel enthalpy is described using the subchannel code, neglecting any local distribution within the subchannel. This leads to the necessity to introduce "memory" effects into CHF correlations based on local conditions. The TONG factor is not used in an isolated manner in PWR CHF correlations. Additional factors describing a type of memory effect are typically included, thus compensating the shortcomings of the TONG factor. Examples are:

- Active length used in the BWU-Z CHF correlation [3]
- Inlet enthalpy used in the BHTP CHF correlation [4]
- Heated length used in the ACH-2 CHF correlation [5]

In all these cases the TONG factor or a similar non-uniform factor was compensated by including additional dependencies. The advantage of using [ ] is the direct connection to flow related quantities, rather than geometrical quantities (heated length) or inlet conditions (inlet enthalpy).

Heated length

As indicated above, an experimental data set was used to identify the parameters that have impact on CHF. Evaluations performed using this data set did not identify any impact of the test assembly heated length on the measured CHF. Therefore, heated length is not a parameter in ORFEO correlation form.

Hydraulic diameter / Equivalent heated diameter

Hydraulic diameter and equivalent heated diameter are generally used to capture the effects of different subchannel types (e.g., unit vs. guide tube) and different fuel assembly geometries. In the ORFEO correlation form these two effects are separated. As indicated above, the guide tube impact is incorporated via a dedicated parameter. The differences in fuel assembly geometry (rod diameter, rod pitch, etc.) are captured by developing adequate fuel design specific multipliers (F_{SPACER}).

ORFEO CHF correlation form

The functional form of the ORFEO CHF correlation is the following:

$$CHF = \frac{F_{BASE}\left(P, G, X, Z_{BO}\right) \cdot F_{SPACER}\left(P, G, X, Geometry\right)}{FNU}$$

where:

F_{BASE} - CHF general representation term, based on local conditions, MW/m^2

F_{SPACER} - fuel design specific multiplier, based on grid specific designs

FNU - axial power factor, accounts for non-uniform axial power profiles

F_{BASE} term

The F_{BASE} term incorporates the generic dependency on local thermal-hydraulic conditions (pressure, mass flux, effective quality) and burnout length (Z_{BO}). The form of the F_{BASE} term is:

where:

The normalized pressure and mass flux are defined:

where:

P - system pressure (MPa)

G - local (subchannel) mass flux $\left(\frac{kg}{m^2 \cdot s}\right)$

The values of the “a” and “b” coefficients are listed in Table 6-1.

The quality functions are defined as follows:

where X is the effective quality.

The effective quality incorporates the burnout length term and is defined:

where:

X_{eq} - local (subchannel) equilibrium quality (-)

Z_{BO} - burnout length (m)

Table 6-1 Coefficients in F_{BASE} term

F_{SPACER} term

The F_{SPACER} term incorporates the specific CHF dependency of the fuel assembly geometry and spacer grid design. The form of the F_{SPACER} term is the same for both correlations, ORFEO-GAIA and ORFEO-NMGRID; however, the coefficients are different. The form of the F_{SPACER} term is the following:

[ ]

The distance-to-grid effect is modeled using [ ] as follows:

[ ]

where:

dg - distance-to-grid (distance from the elevation where CHF is calculated to the elevation of the bottom edge of the upstream grid; see Figure 6-3) (m).

$l_{grid,1}$ - decay length coefficient defined in Table 6-4 for ORFEO-GAIA and Table 6-6 for ORFEO-NMGRID (m).

All structural and intermediate grids (with or without mixing vanes) are included when deriving the F_{GRID} term.

The guide tube impact accounts for the difference in measured CHF performance between the guide tube subchannel and the unit subchannel of a grid:

[ ]

where rtg is [ ]

The effect of grid spacing is modeled using [ ]

The grid spacing term is calculated as follows:

[ ]

where:

gsp - grid spacing (lower edge-to-lower edge distance between two consecutive grids, see Figure 6-3) (m).

$l_{grid,2}$ - decay length coefficient defined in Table 6-4 for ORFEO-GAIA and Table 6-6 for ORFEO-NMGRID (m).

The grid spacing is based on [ ] this includes the case when CHF is calculated in the span that contains the end of heated length. When CHF is calculated [ ]

The coefficients in the F_{SPACER} term are grid design specific. The calculation process and resulting values of the coefficients in the F_{SPACER} term for the ORFEO-GAIA and ORFEO-NMGRID correlations are described in Sections 6.3 and Section 6.4, respectively.

FNU term

The ORFEO correlation form incorporates an axial power factor, FNU to describe the memory effects observed when comparing CHF test data based on uniform versus non-uniform axial power profiles. The axial power factor is based on Tong's formulation [12, Chapter 5.3.2.1]:

$$FNU\left(l_{DNB}\right)=\frac{K}{\varphi\left(l_{DNB}\right)\cdot\left(1-e^{-K\cdot l_{DNB}}\right)}\int_0^{l_{DNB}}\varphi(z)\cdot e^{-K\cdot\left(l_{DNB}-z\right)}dz$$

$$K=\frac{b_1\cdot\left(1-X_{eq}\right)^{b_2}}{\left(\frac{G}{1000}\right)^{b_3}}$$

where:

l_{DNB} - elevation where CHF is calculated (m)

z - elevation (m)

$\varphi(z)$ - local heat flux $\left(\frac{MW}{m^2}\right)$

In the above equation, the integration interval starts at the beginning of the heated length. [ ] The coefficients of the empirical factor K are fitted to reflect the overall description of non-uniform axial power profiles in the ORFEO correlation form via [ ] The values of the "b" coefficients in FNU term are listed in Table 6-2.

Table 6-2 Coefficients in FNU term

[ ]

[ ] It can be viewed as an initial approximation of the CHF performance of a particular grid design. A preliminary value for F_{SPACER} was used in order to allow the fitting of F_{BASE} and FNU. The F_{SPACER} term can be viewed as an adjustment applied to the generic part of the ORFEO correlation in order to reflect the CHF performance of a particular grid design. The fitting process of the F_{SPACER} term is based on CHF test data collected for that particular grid design. The correlation generated in this manner provides an adequate representation of the measured CHF performance from the tests used to fit the F_{SPACER} term.

Sections 6.3 and 6.4 describe the development process for the ORFEO-GAIA and ORFEO-NMGRID correlations, respectively.

6.3 *ORFEO-GAIA CHF correlation*

The CHF test data set for the mixing grids (GAIA structural and IGM) is described in Table B-1. In order to develop and validate the ORFEO-GAIA correlation, the data set is divided as follows:

Table 6-3 provides the number of statepoints from each test in each partition. The partitions were generated using a random selection process.

Table 6-3 Number of statepoints in the defining and validation data sets for ORFEO-GAIA correlation

Figure 6-4, Figure 6-5 and Figure 6-6 show the distribution of defining and validation data sets in terms of pressure, mass flux and equilibrium quality at the MDNBR location as predicted by the ORFEO-GAIA CHF correlation. The two data sets provide an equivalent coverage of the test domain. Each partition therefore provides an adequate representation of the range of applicability and is sufficiently large to assess the correlation uncertainty.

Figure 6-4 Distribution of the defining and validation data sets for the ORFEO-GAIA correlation (mass flux vs. pressure)

Figure 6-5 Distribution of the defining and validation data sets for the ORFEO-GAIA correlation (equilibrium quality vs. pressure)

Figure 6-6 Distribution of the defining and validation data sets for the ORFEO-GAIA correlation (equilibrium quality vs. mass flux)

[ ]

The defining data set was evaluated using COBRA-FLX and local thermal-hydraulic conditions were generated for each statepoint (Table B-2). The coefficients in the F_{SPACER} term of the ORFEO-GAIA correlation were optimized via successive iterations using the algorithm described in Appendix C. The optimized set of coefficients is listed in Table 6-4. The coefficient optimization process is based on [ ] Consistent with this approach, the statistical analysis performed in Section 7.1 is based on [ ]

Table 6-4 Coefficients in F_{SPACER} term for ORFEO-GAIA correlation

6.4 *ORFEO-NMGRID CHF correlation*

The CHF test data set for the non-mixing grids is described in Table B-3. In order to develop and validate the ORFEO-NMGRID correlation, the data set is divided as follows:

Table 6-5 provides the number of statepoints from each test in each partition. The partitions were generated using a random selection process.

Table 6-5 Number of statepoints in the defining and validation data sets for ORFEO-NMGRID correlation

Figure 6-7, Figure 6-8 and Figure 6-9 show the distribution of defining and validation data sets in terms of pressure, mass flux and equilibrium quality at the MDNBR location as predicted by the ORFEO-NMGRID CHF correlation. The two data sets provide an equivalent coverage of the test domain. Each partition therefore provides an adequate representation of the range of applicability and is sufficiently large to assess the correlation uncertainty.

Figure 6-7 Distribution of the defining and validation data sets for the ORFEO-NMGRID correlation (mass flux vs. pressure)

Figure 6-8 Distribution of the defining and validation data sets for the ORFEO-NMGRID correlation (equilibrium quality vs. pressure)

Figure 6-9 Distribution of the defining and validation data sets for the ORFEO-NMGRID correlation (equilibrium quality vs. mass flux)

[ ]

The defining data set was evaluated using COBRA-FLX and local thermal-hydraulic conditions were generated for each statepoint (Table B-4). The coefficients in the F_{SPACER} term of the ORFEO-NMGRID correlation were optimized via successive iterations using the algorithm described in Appendix C. The optimized set of coefficients is listed in Table 6-6. The coefficient optimization process is based on [ ] Consistent with this approach, the statistical analysis performed in Section 7.2 is based on [ ]

Table 6-6 Coefficients in F_{SPACER} term for ORFEO-NMGRID correlation

The following can be noted regarding the F_{SPACER} coefficients in Table 6-6:

6.5 *Correlation behavior*

Figure 6-10, Figure 6-11 and Figure 6-12 show the ORFEO-GAIA correlation behavior as a function of pressure, mass flux and effective quality, respectively.

Figure 6-13, Figure 6-14 and Figure 6-15 show the ORFEO-NMGIRD correlation behavior as a function of pressure, mass flux and effective quality, respectively.

Two observations apply to correlations' functional behavior. First, there are no discontinuities; second, the functional behavior is consistent with the Groeneveld CHF tables published in [13].

Figure 6-10 Predicted CHF as a function of pressure for ORFEO-GAIA correlation ($gsp = dg = 0.521\ m$)

Figure 6-11 Predicted CHF as a function of mass flux for ORFEO-GAIA correlation ($gsp = dg = 0.521\ m$)

Figure 6-12 Predicted CHF as a function of effective quality for ORFEO-GAIA correlation ($gsp = dg = 0.521\ m$)

Figure 6-13 Predicted CHF as a function of pressure for ORFEO-NMGRID correlation ($gsp = dg = 0.521\ m$)

Figure 6-14 Predicted CHF as a function of mass flux for ORFEO-NMGRID correlation ($gsp = dg = 0.521\ m$)

Figure 6-15 Predicted CHF as a function of effective quality for ORFEO-NMGRID correlation ($gsp = dg = 0.521\ m$)

7.0 CORRELATION ASSESSMENT AND STATISTICAL ANALYSIS

7.1 *ORFEO-GAIA CHF correlation*

7.1.1 Analysis of defining and validation data sets

The ORFEO-GAIA CHF correlation has been developed based on the defining data set described in Section 6.3. The validation data set represents a second set of experimental data that is used to confirm the adequacy of the correlation using data that was not used to fit the correlation.

The validation data set must be confirmed to be poolable with the defining data set, i.e. the correlation should predict the validation data set with approximately the same level of accuracy as the defining data set.

Poolability was checked by performing the following statistical tests:

- Bartlett's [14] (verifies the homogeneity of variances between the two data sets)
- Standard unpaired t-test (verifies the equality of means between the two data sets)

A prerequisite for these tests is that the population is normally distributed. The normality was checked by applying the D' test [15] and the Epps-Pulley test [16]. The null hypothesis for these tests states that the data set is normally distributed. However, it is well known in the open literature and stated in NUREG/CR-4604 ([17], pg. 535) that large data sets often provide false indications that the data sets are not normally distributed due to the statistical tests becoming overly sensitive with increasing data set size. As an alternative to normality tests, the data can be visually verified to be normally distributed by comparison of the data histogram with a normal (Gaussian) curve.

The tests are used at a 5% significance level. The results of these tests are shown in Table 7-1. **[** **]** Figure 7-1 and Figure 7-2 show the histograms of the M/P populations for the defining and validation data sets with the normal distribution curve. **[**

]

Table 7-1 Results of statistical tests applied to the defining and validation data sets for ORFEO-GAIA correlation

Figure 7-1 Histogram of the defining data set for the ORFEO-GAIA correlation

Figure 7-2 Histogram of the validation data set for the ORFEO-GAIA correlation

Table 7-2 compares the statistics for each test campaign. The average M/P and standard deviation values of the defining and validation data sets for each test are reasonably close such that there is no difference in the predictive behavior of the correlation. Any differences are small relative to the experimental uncertainty. Based on the results of tests for homogeneity of variances and equality of means it is concluded that the defining and validation data sets are poolable. Therefore, the correlation adequately describes the statepoints in the validation data set.

Table 7-2 Overall statistics of the defining and validation data sets for the ORFEO-GAIA correlation

Figure 7-3, Figure 7-4, and Figure 7-5 show the distribution of the M/P data as a function of pressure, mass flux, and equilibrium quality. These figures illustrate that the ORFEO-GAIA correlation adequately describes the two data sets.

Figure 7-3 M/P versus pressure for ORFEO-GAIA correlation (defining and validation data sets)

Figure 7-4 M/P versus mass flux for ORFEO-GAIA correlation (defining and validation data sets)

Figure 7-5 M/P versus equilibrium quality for ORFEO-GAIA correlation (defining and validation data sets)

Since the M/P values for the defining and validation data sets were found to be poolable, they were combined together into one data set. [ ] The statistics of the combined data set are shown in Table 7-3.

Table 7-3 Overall statistics of the combined data set for the ORFEO-GAIA correlation

[ ]

Figure 7-6 shows the histogram of the M/P population obtained when evaluating the combined data set with the ORFEO-GAIA correlation. A normal distribution provides a good approximation of the M/P distribution.

Figure 7-6 Histogram of the combined data set for the ORFEO-GAIA correlation

7.1.2 Design limit

The design limit of the ORFEO-GAIA correlation is calculated using Owen's methodology [18]. A design limit that bounds 95% of the data with 95% confidence is calculated via the following:

$$C = \frac{1}{\bar{x} - k(\beta, \gamma, n-1) \cdot s}$$

$$s^2 = s_w^2 + s_a^2$$

$$s_w^2 = \frac{\sum_{i=1}^{k}(n_i - 1)\cdot s_i^2}{\sum_{i=1}^{k}(n_i - 1)}$$

$$s_a^2 = \frac{1}{k-1}\cdot\left(\sum_{i=1}^{k}\left(Y_i - \frac{1}{k}\cdot\sum_{i=1}^{k}Y_i\right)^2\right)$$

where:

$\bar{x}$ - empirical mean of the M/P population

s^2 - total variance

$k(\beta,\gamma,n-1)$ - Owen's coefficient corresponding to the probability β at the level of confidence γ for $n-1$ degrees of freedom

s_w^2 - pooled variance of test series

s_a^2 - variance of test series means

k - number of test series

n_i - number of statepoints in test series i

s_i^2 - variance of test series i

Y_i - mean of test series i

The effective degrees of freedom to be used in the design limit calculation is based on Satterthwaite [20]:

$$n_{eff} = \frac{\left(s_w^2 + s_a^2\right)}{\frac{s_w^4}{n_w} + \frac{s_a^4}{n_a}}$$

where $n_w = n_i - k$ is the number of degrees of freedom within test series and $n_a = k - 1$ is the number of degrees of freedom among test series means.

Owen's coefficient can be calculated by using the mathematical model established by Natrella [19, pg. 2-15]:

$$k(\beta, \gamma, n_{eff}) = \frac{Z_{1-\beta} + \sqrt{Z_{1-\beta}^2 - a \cdot b}}{a}$$

$$a = 1 - \frac{Z_{1-\gamma}^2}{2 \cdot (n_{eff} - 1)}$$

$$b = Z_{1-\beta}^2 - \frac{Z_{1-\gamma}^2}{n_{eff}}$$

where Z is the critical value based on the normal distribution. For $\beta = \gamma = 0.95$, $Z_{1-0.95} = 1.645$.

The design limit is calculated based on the combined CHF test data set listed in Table 7-3. As indicated in the previous section, [

]

The values of the main parameters of the design limit calculation are listed in Table 7-4. When using the standard deviation of [ ] which is based on the total variance of the M/P population, the resulting design limit is [ ] The correlation design limit has to ensure that all sub-regions are adequately protected such that there are no non-conservative sub-regions. The acceptability of this value is confirmed by investigating the distribution of the statepoints that have an M/P value lower than the inverse of the design limit between pressure, mass flux, equilibrium quality, and the CHF tests.

The results show [ ] statepoints below the design limit with the majority of these distributed as follows:

[ ]

Based on the number and distribution of statepoints below the design limit, non-conservative sub-regions may exist in these ranges. Therefore the design limit is recalculated using the largest standard deviation of all sub-region ranges (Table 7-5, Table 7-6 and Table 7-7) instead of the standard deviation based on the total variance of the combined data set. This value [ ] corresponds to [ ] and is termed the “bounding standard deviation” in Table 7-4. The resulting correlation design limit is [ ]

Table 7-4 Statistical parameters and design limit for ORFEO-GAIA correlation

Sub-regions are again investigated to ensure the design limit is conservative over the entire application range.

Table 7-5, Table 7-6 and Table 7-7 show the distribution of the statepoints that have an M/P value lower than the inverse of the design limit between the pressure, mass flux and equilibrium quality ranges. No pressure or equilibrium quality ranges exhibit an unexpected number of statepoints below the design limit. [

]

Table 7-5 Distribution of statepoints below the ORFEO-GAIA correlation design limit by pressure ranges

Table 7-6 Distribution of statepoints below the ORFEO-GAIA correlation design limit by mass flux ranges

Table 7-7 Distribution of statepoints below the ORFEO-GAIA correlation design limit by equilibrium quality ranges

Figure 7-7 M/P versus pressure for the ORFEO-GAIA correlation for [ ]

The combined data set of the ORFEO-GAIA correlation is further investigated based on the geometric characteristics of the test assemblies. Table 7-8, Table 7-9 and Table 7-10 show the mean and standard deviation values of the M/P population based on subchannel, axial power profile, and grid type. All categories are adequately described without any bias. For each category a t-test was performed to verify the equality of means. The t-test is used at a 5% significance level. A test for homogeneity of variances is not necessary since the t-test accounts for non-equal variances. The statistical analysis results are shown in Table 7-11. Each pair of data sets passes the t-test, hence the means are statistically indistinguishable from each other.

Table 7-8 Overall statistics of the combined data set for the ORFEO-GAIA correlation by subchannel type

Table 7-9 Overall statistics of the combined data set for the ORFEO-GAIA correlation by axial power profile type

Table 7-10 Overall statistics of the combined data set for the ORFEO-GAIA correlation by grid type

Table 7-11 Results of statistical tests applied to ORFEO-GAIA combined data set (subchannel, axial power profile and grid type)

[ ]

Figure 7-8 through Figure 7-12 show the M/P data as a function of pressure, mass flux, equilibrium quality, distance-to-grid and grid spacing, respectively. The ORFEO-GAIA correlation adequately predicts the combined data set [

]

Figure 7-8 M/P versus pressure for ORFEO-GAIA correlation (combined data set)

Figure 7-9 M/P versus mass flux for ORFEO-GAIA correlation (combined data set)

Figure 7-10 M/P versus equilibrium quality for ORFEO-GAIA correlation (combined data set)

Figure 7-11 M/P versus distance-to-grid for ORFEO-GAIA correlation (combined data set)

Figure 7-12 M/P versus grid spacing for ORFEO-GAIA correlation (combined data set)

[ ]

7.1.3 [ ]

[ ]

Figure 7-13 M/P versus pressure for ORFEO-GAIA correlation

[ ]

Figure 7-14 M/P versus mass flux for ORFEO-GAIA correlation

[ ]

Figure 7-15 M/P versus equilibrium quality for ORFEO-GAIA correlation

[ ]

Figure 7-16 M/P versus burnout length for ORFEO-GAIA correlation

[ ]

7.1.4 Application range

The application range for the ORFEO-GAIA correlation is established based on the coverage of the CHF test data set in terms of pressure, mass flux and equilibrium quality. The CHF tests are designed to cover the parameter ranges required by safety analysis applications. Figure 7-17, Figure 7-18, and Figure 7-19 show the distribution of the combined data set (including [ ]) in terms of pressure, mass flux, and equilibrium quality at the MDNBR location as predicted by the ORFEO-GAIA correlation.

The application range (local thermal-hydraulic conditions) for the ORFEO-GAIA CHF correlation is listed in Table 7-12. No lower bound is imposed on the quality range.

Figure 7-17 Distribution of the combined data set [ ] for the ORFEO-GAIA correlation (mass flux vs. pressure)

Figure 7-18 Distribution of the combined data set [ ] for the ORFEO-GAIA correlation (equilibrium quality vs. pressure)

Figure 7-19 Distribution of the combined data set [ ] for the ORFEO-GAIA correlation (equilibrium quality vs. mass flux)

Table 7-12 Range of application for ORFEO-GAIA CHF correlation (local thermal-hydraulic conditions)

Parameter	Units	Minimum value	Maximum value
Pressure	MPa	9.97	17.45
	psia	1446.0	2530.9
Mass flux	kg/m^2s	679.8	4323.4
	$Mlbm/ft^2hr$	0.5012	3.1878
Equilibrium quality	fraction	---	0.7992

7.2 *ORFEO-NMGRID CHF correlation*

7.2.1 Analysis of defining and validation data sets

The ORFEO-NMGRID CHF correlation has been developed using the same methodology described in Section 7.1 for the ORFEO-GAIA correlation and is based on the data set described in Section 6.4.

As described in Section 7.1.1, the validation data set must be confirmed to be poolable with the defining data set and the Bartlett's [14] and t-test are used for this calculation. A prerequisite for these tests is that the population is normally distributed. The normality can be verified by applying the D' test [15] and the Epps-Pulley test [16]. The tests are used at a 5% significance level. As shown in Table 7-13, [

]

Table 7-13 Results of statistical tests applied to the defining and validation data sets for ORFEO-NMGRID correlation

[ ]

Table 7-14 compares the statistics for each test campaign. The average M/P and standard deviation values of the defining and validation data sets for each test are reasonably close such that there is no difference in the predictive behavior of the correlation. Any differences are small relative to the experimental uncertainty. Based on the results of tests for homogeneity of variances and equality of means it is concluded that the defining and validation data sets are poolable. Therefore, the correlation adequately describes the statepoints in the validation data set.

Table 7-14 Overall statistics of the defining and validation data sets for the ORFEO-NMGRID correlation

Figure 7-20, Figure 7-21, and Figure 7-22 show the distribution of the M/P population as a function of pressure, mass flux, and equilibrium quality. These figures illustrate that the ORFEO-NMGRID correlation adequately describes the two data sets.

Figure 7-20 M/P versus pressure for ORFEO-NMGRID correlation (defining and validation data sets)

Figure 7-21 M/P versus mass flux for ORFEO-NMGRID correlation (defining and validation data sets)

Figure 7-22 M/P versus equilibrium quality for ORFEO-NMGRID correlation (defining and validation data sets)

Since M/P values for the defining and validation data sets were found to be poolable, they were combined together into one data set for use in the design limit calculation.

[ ] The statistics of the combined data set is shown in Table 7-15.

Table 7-15 Overall statistics of the combined data set for the ORFEO-NMGRID correlation

[ ]

Figure 7-23 displays the histogram of the M/P population obtained when evaluating the combined data set with the ORFEO-NMGRID correlation. A normal distribution provides a good approximation of the M/P distribution.

Figure 7-23 Histogram of the combined data set for the ORFEO-NMGRID correlation

7.2.2 Design limit

The design limit of the ORFEO-NMGRID correlation is calculated using Owen's methodology [18]. The same method described in Section 7.1.2 for the ORFEO-GAIA correlation is applied here.

The main parameters used in calculating the design limit are provided in Table 7-16. When using the total M/P data set standard deviation [ ] the resulting design limit is [ ] The correlation design limit has to ensure that all sub-regions are adequately protected i.e., there are no non-conservative sub-regions.

The results show [ ] statepoints below the design limit with a majority distributed as follows:

[ ]

Based on the number of statepoints below the design limit, non-conservative sub-regions may exist in these ranges. This issue is resolved by recalculating the design limit using the largest standard deviation of all sub-regions (see Table 7-17, Table 7-18 and Table 7-19) instead of the standard deviation based on the total combined data set. This value [ ] corresponds to the [ ] and is termed the "bounding standard deviation" in Table 7-16. The resulting correlation design limit is [ ]

Table 7-16 Statistical parameters and design limit for ORFEO-NMGRID correlation

Sub-regions are again investigated to ensure the design limit is conservative over the entire application range.

Table 7-17, Table 7-18 and Table 7-19 show the distribution of the statepoints that have an M/P value lower than the inverse of the design limit between the pressure, mass flux and equilibrium quality ranges. No individual range exhibits an unexpected number of statepoints below the correlation design limit.

Table 7-17 Distribution of statepoints below the ORFEO-NMGRID correlation design limit by pressure ranges

Table 7-18 Distribution of statepoints below the ORFEO-NMGRID correlation design limit by mass flux ranges

Table 7-19 Distribution of statepoints below the ORFEO-NMGRID correlation design limit by equilibrium quality ranges

The combined data set of the ORFEO-NMGRID correlation is further investigated based on the geometric characteristics of the test assemblies. Table 7-20 and Table 7-21 show the mean and standard deviation values of the M/P population based on subchannel type and axial power profile. All categories are adequately described without any bias. For each category the statistics are compared, a t-test is performed to verify the equality of means. The t-test is used at a 5% significance level. A test for homogeneity of variances is not necessary since the t-test accounts for non-equal variances. The statistical analysis results are shown in Table 7-22. Each pair of data sets passes the t-test; hence the means are statistically indistinguishable from each other.

Table 7-20 Overall statistics of the combined data set for the ORFEO-NMGRID correlation by subchannel type

Table 7-21 Overall statistics of the combined data set for the ORFEO-NMGRID correlation by axial power profile type

Table 7-22 Results of statistical tests applied to ORFEO-NMGRID combined data set (subchannel and axial power profile type)

Figure 7-24, Figure 7-25, Figure 7-26, Figure 7-27 and Figure 7-28 show the M/P distribution as a function of pressure, mass flux, equilibrium quality, distance-to-grid and grid spacing, respectively. The ORFEO-NMGRID correlation predictions of the combined data set [

] exhibit good behavior.

Figure 7-24 M/P versus pressure for ORFEO-NMGRID correlation (combined data set)

[

]

Figure 7-25 M/P versus mass flux for ORFEO-NMGRID correlation (combined data set)

Figure 7-26 M/P versus equilibrium quality for ORFEO-NMGRID correlation (combined data set)

Figure 7-27 M/P versus distance-to-grid for ORFEO-NMGRID correlation (combined data set)

Figure 7-28 M/P versus grid spacing for ORFEO-NMGRID correlation (combined data set)

7.2.3 Application range

The application range for the ORFEO-NMGRID correlation is established based on the coverage of the CHF test data set in terms of pressure, mass flux and equilibrium quality. The CHF tests are designed to cover the parameter ranges required by safety analysis applications. Figure 7-29, Figure 7-30, and Figure 7-31 show the distribution of the combined data set in terms of pressure, mass flux, and equilibrium quality at the MDNBR location as predicted by the ORFEO-NMGRID correlation.

The application range (local thermal-hydraulic conditions) for the ORFEO-NMGRID CHF correlation is listed in Table 7-23. No lower bound is imposed on the quality range.

Figure 7-29 Distribution of the combined data set for the ORFEO-NMGRID correlation (mass flux vs. pressure)

Figure 7-30 Distribution of the combined data set for the ORFEO-NMGRID correlation (equilibrium quality vs. pressure)

Figure 7-31 Distribution of the combined data set for the ORFEO-NMGRID correlation (equilibrium quality vs. mass flux)

Table 7-23 Range of application for ORFEO-NMGRID CHF correlation (local thermal-hydraulic conditions)

Parameter	Units	Minimum value	Maximum value
Pressure	MPa	2.01	17.46
	psi	291.5	2532.4
Mass flux	kg/m^2s	406.5	4826.0
	$Mlbm/ft^2hr$	0.2997	3.5584
Equilibrium quality	fraction	---	0.8769

7.2.4 Application to the mixing grid CHF data set

In addition to the data set analyzed in Section 7.2.1, the ORFEO-NMGRID correlation is used for the mixing grid region of the GAIA fuel assembly design outside of the application range of the ORFEO-GAIA correlation, in particular at pressures lower than 9.97 MPa. ORFEO-NMGRID correlation is applied to a mixing grid CHF test data set consisting of the combined data set defined in Section 7.1.1 and low pressure CHF test data collected for the mixing grids. Note that the low pressure CHF test data is not listed in Appendix B. Table 7-24 shows the overview of the statistics of this mixing grid CHF data set evaluated with the ORFEO-NMGRID correlation. Figure 7-32, Figure 7-33 and Figure 7-34 show the dependency of the M/P distribution on pressure, mass flux and equilibrium quality. The evaluation demonstrates that the ORFEO-NMGRID correlation can be applied conservatively with the design limit of [ ] to the GAIA fuel assembly design on the full application range defined in Table 7-23. The [ ] design limit bounds all statepoints.

Table 7-24 Overall statistics of the mixing grid CHF data set evaluated with the ORFEO-NMGRID correlation

[ ]

Figure 7-32 M/P versus pressure for the mixing grid CHF data set evaluated with the ORFEO-NMGRID correlation

Figure 7-33 M/P versus mass flux for the mixing grid CHF data set evaluated with the ORFEO-NMGRID correlation

Figure 7-34 M/P versus equilibrium quality for the mixing grid CHF data set evaluated with the ORFEO-NMGRID correlation

8.0 GEOMETRIC COMPARISON OF PRODUCTION GRID TO TESTED GRID

For all CHF testing (by all vendors), the production assembly is simulated using electrically heated rods in place of nuclear fuel rods. The part of the assembly that affects the CHF lies between the beginning of heated length and the end of heated length (Figure 2-1). The lower end fitting and upper end fitting have no effect on the CHF and are not included in the test assembly.

The GAIA production assembly is based on a 17-by-17 matrix. The CHF performance of the two axial regions (with mixing and non-mixing grids) on the GAIA production assembly is derived based on CHF testing performed on 5-by-5 test assemblies. The radial configurations of the test assemblies are described in Section 4.2.2. This is consistent with the approach used for previous CHF correlations (e.g., BWU-Z and ACH-2 approved by the U.S. NRC in [3] and [5], respectively).

The GAIA production grid exhibits some minor geometric variations from the tested geometries that go beyond manufacturing tolerances.

These variations either do not affect the CHF performance or marginally enhance the CHF performance. The flow field is negligibly impacted by the described variations because:

This justification indicates that the existing minor geometric variations do not degrade the CHF performance of the GAIA production grid. Therefore, the CHF test program adequately represents the CHF performance of the GAIA production grid.

Figure 8-1 GAIA structural grid - guide tube configurations

Figure 8-2 Depiction of various unit cell flap configurations

Figure 8-3 Vane slots on GAIA grid

9.0 QUALITY ASSURANCE PROGRAM (QAP)

9.1 *QAP specific to correlation development*

The ORFEO-GAIA and ORFEO-NMGRID correlations are developed and maintained under a quality assurance program that meets the regulatory requirements of 10 CFR Part 50 Appendix B.

9.2 *QAP specific to GAIA CHF testing*

The testing organization (that operates the KATHY loop) is treated as a supplier for testing and data that is subject to 10 CFR Part 50 Appendix B. As such, periodic audits are performed on the quality assurance program of the supplier to ensure that it remains in compliance with the quality assurance requirements. The frequency of the audits is based on the compliance history of the supplier and the frequency of use of the supplier. Certification of the supplier is provided for a specified period of time.

10.0 REFERENCES

1. Standard Review Plan for the Review of Safety Analysis Reports for Nuclear Plants: LWR Edition, NUREG-0800, March 2007
2. R. H. Wilson, D. A. Farnsworth and R. H. Stoudt, "BWC Correlation of Critical Heat Flux", BAW-10143P-A, Babcock & Wilcox, April 1985
3. D. A. Farnsworth and G. A. Meyer, "The BWU Critical Heat Flux Correlations," BAW-10199P-A, Rev. 0, Framatome Technologies, February 1998
4. D. A. Farnsworth and R. L. Harne, "BHTP DNB Correlation Applied with LYNXT", BAW-10241(P)(A), Rev. 1, Framatome ANP, Inc., July 2005
5. D. A. Farnsworth and R. L. Harne, "The ACH-2 CHF Correlation for the U.S. EPR", ANP-10269P-A, Rev. 0, AREVA NP Inc., December 2007
6. C. Herer, A. Beisiegel, P. Imbert, D.A. Farnsworth and F. Burtak, "Comparison of PWR Fuel Assembly CHF Tests Obtained at Three Different Test Facilities", NURETH-11, October 2005
7. "COBRA-FLX: A Core Thermal-Hydraulic Analysis Code", ANP-10311P-A, AREVA NP Inc., January 2013
8. J. G. Collier and J. R. Thome, "Convective Boiling and Condensation", 3rd Edition, Clarendon Press, Oxford, 1994
9. C. F. Fighetti and D. G. Reddy, "Parametric Study of CHF Data, Volume 2: A Generalized Subchannel CHF Correlation for PWR and BWR Fuel Assemblies", NP-2609, Volume 2, EPRI, January 1983
10. D.C. Groeneveld, J.Q. Shan, A.Z. Vasi, L.K.H. Leung, A. Durmayaz, J. Yang, S.C. Cheng and A. Tanase, "The 2006 CHF Look-up Table", Nuclear Engineering and Design 237 (2007) 1909–1922

11. M. Lee, "A Critical Heat Flux Approach for Square Rod Bundles Using the 1995 Groeneveld CHF Table and Bundle Data of Heat Transfer Research Facility", Nuclear Engineering and Design 197 (2000) 357–374

12. L. S. Tong and Y. S. Tang, "Boiling Heat Transfer and Two-Phase Flow", 2nd Edition, Taylor and Francis, 1997

13. D.C. Groeneveld et al., "The 1996 look-up table for critical heat flux in tubes", Nuclear Engineering and Design 163 (1996) 1-23

14. G. W. Snedecor and W. G. Cochran, "Statistical Methods", 8th Edition, Iowa State University Press, 1989

15. R. B. D'Agostino, "An Omnibus Test of Normality for Moderate and Large Size Samples", Biometrika, Vol. 58, 1971

16. T. W. Epps and L. B. Pulley, "A test for normality based on the empirical characteristic function", Biometrika 70, 723–726, 1983

17. Statistical Methods for Nuclear Material Management, NUREG/CR-4604, December 1988

18. D.B. Owen, "Factors for One-sided Tolerance Limits and for Variable Sampling Plans", SCR-607, Sandia Corporation, March 1963

19. M.G. Natrella, "Experimental Statistics", Dover Publications Inc., 2005

20. F.E. Satterthwaite, "An Approximate Distribution of Estimates of Variance Components", Biometrics Bulletin, Vol. 2, No. 6, 1946

APPENDIX A. AXIAL GEOMETRY OF TEST ASSEMBLIES

Figure A-1 Axial geometry of CHF test K7100

Figure A-2 Axial geometry of CHF test K7300

Figure A-3 Axial geometry of CHF test K760x

Figure A-4 Axial geometry of CHF test K770x

Figure A-5 Axial geometry of CHF test K780x

Figure A-6 Axial geometry of CHF test K8100

Figure A-7 Axial geometry of CHF test K820x

Figure A-8 Axial geometry of CHF test K830x

Figure A-9 Axial geometry of CHF test K840x

Figure A-10 Axial geometry of CHF test K8601

Figure A-11 Axial geometry of CHF test AR6

Figure A-12 Axial geometry of CHF test AR7

Figure A-13 Axial geometry of CHF test AR8

Figure A-14 Axial geometry of CHF test AR9

Figure A-15 Axial geometry of CHF test AR11

Figure A-16 Axial geometry of CHF test AR12

Figure A-17 Axial geometry of CHF test K6800

Figure A-18 Axial geometry of CHF test K8500

Figure A-19 Axial geometry of CHF test O1500

Figure A-20 Axial geometry of CHF test SI110/SI111

Figure A-21 Axial geometry of CHF test SI190

Figure A-22 Axial geometry of CHF test SI210

Figure A-23 Axial geometry of CHF test SI340

APPENDIX B: CHF TEST DATA

Table B-1 Test assembly conditions for mixing grid tests

Table B-2 Local conditions from COBRA-FLX simulations for mixing grid tests

Table B-3 Test assembly conditions for non-mixing grid tests

Table B-4 Local conditions from COBRA-FLX simulations for non-mixing grid tests

APPENDIX C. CORRELATION FITTING PROCESS

Figure C-1 Flow chart of the genetic algorithm

Figure C-2 Three stage correlation fitting process